2014

There Can Be Turbulence in Microfluidics at Low Reynolds Number

Guiren Wang
University of South Carolina - Columbia, wanggu@cec.sc.edu

F. Yang

Wei Zhao
University of South Carolina - Columbia, zhao9@engr.sc.edu

Publication Info

Published in *Lab on a Chip*, Volume 14, Issue 8, 2014, pages 1452-1458.

Wang, G. R., Yang, F., & Zhao, W. (2014). There can be turbulence in microfluidics at low Reynolds number. *Lab on a Chip*, 14(8), 1452-1458.
http://dx.doi.org/10.1039/C3LC51403J

Lab on a Chip

PAPER

View Article Online
View Journal | View Issue

Cite this: *Lab Chip*, 2014, **14**, 1452

There can be turbulence in microfluidics at low Reynolds number

G. R. Wang,*[ab] Fang Yang†[a] and Wei Zhao†[a]

Received 18th December 2013,
Accepted 23rd January 2014

DOI: 10.1039/c3lc51403j

www.rsc.org/loc

Turbulence is commonly viewed as a type of macroflow, where the Reynolds number (Re) has to be sufficiently high. In microfluidics, when Re is below or on the order of 1 and fast mixing is required, so far only chaotic flow has been reported to enhance mixing based on previous publications since turbulence is believed not to be possible to generate in such a low Re microflow. There is even a lack of velocimeter that can measure turbulence in microchannels. In this work, we report a direct observation of the existence of turbulence in microfluidics with Re on the order of 1 in a pressure driven flow under electrokinetic forcing using a novel velocimeter having ultrahigh spatiotemporal resolution. The work could provide a new method to control flow and transport phenomena in lab-on-a-chip and a new perspective on turbulence.

1. Introduction

One important issue in microfluidics is the relatively slow mixing of two fluids due to laminar flow at low Reynolds number (Re). However, in many cases, *e.g.* studying the mechanism of protein folding which involves fast kinetics, rapid mixing is very important and highly demanded. In macroflows, where Re is relatively high, mixing can usually be enhanced by forcing flow to be turbulent. Although there can be elastic turbulence in polymer solutions at low Re,[1] it is conventionally believed that the flow in microfluidics, where typical Re is on the order of 1 or lower and the fluids are often approximately seen as Newtonian, can only be laminar[2,3] and cannot be turbulent.[4–7] There is even no available velocimeter that can measure turbulence in microfluidics.[8] According to a recent review, Chang and Yang[9] implied that, so far, many efforts have been made to enhance mixing in microfluidics, *e.g.* using sufficiently high DC or AC voltage to force flow in a microchannel based on electrokinetic instability,[10–15] but the forced flows in these studies are chaotic advection, not turbulence.

Can there be turbulence in a microchannel with Re on the order of 1? To address this issue, we have to know first what turbulence is. Although it is difficult to give an accurate definition of turbulence, there are some common features in turbulence:[16] fast diffusion, random motion, high dissipation rate, continuous flow, multiscale eddies, 3-D flow and high Re. Based on these features, common knowledge is that the critical Reynolds number—Re_c—is 2100–2300 in pipe flow. In microfluidics, turbulence is hard to be generated unless the pressure head is high enough.[17,18] As we know, Re_c in microchannels is similar to that in macroflows, although debates exist.[19] In macroflows, we have realized turbulence and ultrafast mixing at relatively low Re based on receptivity.[20,21] In the present work, we demonstrate that turbulence can be achieved in an electrokinetically forced pressure-driven flow in microchannels with Re on the order of 1.

2. Principle of generating and measuring turbulence in microfluidics at low Re

In the present work, the principle of generating turbulence in microfluidics at low Re is described below. The dynamical process of electrokinetics can be described by the Navier–Stokes equation as

$$\rho\left(\frac{\partial \vec{u}}{\partial t}+\vec{u}\cdot\nabla\vec{u}\right)=\nabla p+\eta\nabla^2\vec{u}+\vec{F}_e \quad (1)$$

where ρ, $\vec{u}$, p, η and $\vec{F}_e$ are the fluid density, flow velocity, pressure, dynamic viscosity and electrical body force, respectively. $\vec{F}_e=\rho_f\vec{E}$, where $\vec{E}$ is the electric field and $\rho_f=-\varepsilon\vec{E}\cdot\nabla\sigma/\sigma$ denotes the initial free charge density in solution,[11] where ε is the permittivity of the electrolyte, σ is the electric conductivity of the medium and $\nabla\sigma$ is the conductivity gradient. In pressure driven flows at low Re in microfluidics, usually the pressure term ∇p alone cannot surpass the viscous force $\eta\nabla^2\vec{u}$ to produce a large inertial term and generate turbulence; further, the flows should be laminar. To overcome the strong viscous force, one can introduce other body forces to

[a] *Department of Mechanical Engineering, University of South Carolina, Columbia, USA. E-mail: guirenwang@sc.edu*
[b] *Biomedical Engineering Program, University of South Carolina, Columbia, USA*
† These authors have made equal contribution to this work.

balance the influence of the viscous force. In microfluidics, this can be realized by generating a relatively strong electric body force $\vec{F}_e$ on the fluid. By increasing ρ_f through management of the given $\vec{E}$ and $\nabla\sigma$, the ratio between the electric body force and viscous force, *i.e.* the electric Grashof number Gr_e, can be increased.

Gr_e is also the ratio of electric Rayleigh number Ra_e to Schmidt number Sc,[22] with $Ra_e = \varepsilon w^2 E_0^2(\sigma_2 - \sigma_1)/\sigma_1\eta D_e$ and $Sc = \eta/\rho D_e$, where D_e is effective diffusivity, σ_1 and σ_2 are the conductivities of the two streams, w is the width of the channel at the entrance, and $E_0 = V/\sqrt{2}w$ is the root-mean square value of the nominal electric field strength (where V is the applied peak-to-peak voltage between the two electrodes). Since for a given fluid, Sc is constant, Ra_e has been used to represent the ratio of electrical stress to viscous forces. The critical Ra_e, beyond which the flow becomes unstable, depends on its definition and flow management and can be in the range of $10–10^5$.[23]

In electrokinetics, if the inertial and electric forces are balanced and both are larger than the viscous force, a corresponding characteristic velocity scaled by $U_e = \sqrt{\varepsilon(\sigma_2 - \sigma_1)E_0^2/\rho\sigma}$ (ref. 22) can be concluded. For a given length scale l_e, we have the convective time scale $\tau_e = l_e/U_e$, which in turn is much smaller than the related viscous diffusion time $\tau_d = \rho l_e^2/\eta$ for large l_e. In this case, the viscous effect is negligible compared with the convection effect, which due to shear stress and nonlinear effects can generate smaller scale structures. As l_e becomes smaller, τ_d decreases faster than τ_e. At sufficiently small l_e, where $\tau_d = \tau_e$, the viscous effect is directly balanced by the inertial and electric effects, giving the possibly smallest length scale as $l_{de} = \sqrt{\eta^2\sigma_1/\rho\varepsilon E_0^2(\sigma_2 - \sigma_1)}$. Clearly if $(\sigma_2 - \sigma_1)E_0^2$ is sufficiently large, l_{de} can be much smaller (*e.g.* more than one order) than the channel width. Hence, there could be multiple scales, a feature of turbulence. This could give the flow enough spatial-temporal space, if Ra_e is sufficiently high, for a continuous power spectrum of turbulence to be developed, even though Re is still very low.

Previously, in electrokinetic microfluidics, the electrodes are commonly placed at the inlet and outlet of the channel to induce electrokinetic instability and increase mixing in the flow.[11,12] In such a type of micromixer, since $\vec{E}$ is perpendicular to $\nabla\sigma$, the electric charge density ρ_f and the corresponding $\vec{F}_e$ are very small. The corresponding mixing is achieved by amplifying the original small disturbance at the interface between the two fluid streams due to electrokinetic instability.[11] In the present work, four methods were explored to achieve turbulence. (1) We use two conductive sidewalls to force the flow. In this management, for a given $\vec{E}$ and $\nabla\sigma$, ρ_f is increased by arranging $\vec{E}$ to be nearly parallel to $\nabla\sigma$. In the present setup, $\vec{E}$ is almost parallel to $\nabla\sigma$, and a strong transverse force component $\vec{F}_{ey}$ of $\vec{F}_e$ is created to compete with the viscous force. (2) The microchannel is made of a diffuser with a small angle to introduce a non-uniform electric field in the x-direction, and thus, a streamwise force $\vec{F}_{ex}$ as well (see Fig. 1(a)). The $\vec{F}_{ex}$ near the surfaces of the two electrode are in opposite directions because of the reverse electric fields in the bulk flow direction. Synergy of these forces will create more local shear and a secondary flow, which in turn can generate and enhance 3-D turbulent flow even at low Re because of incompressibility. (3) There

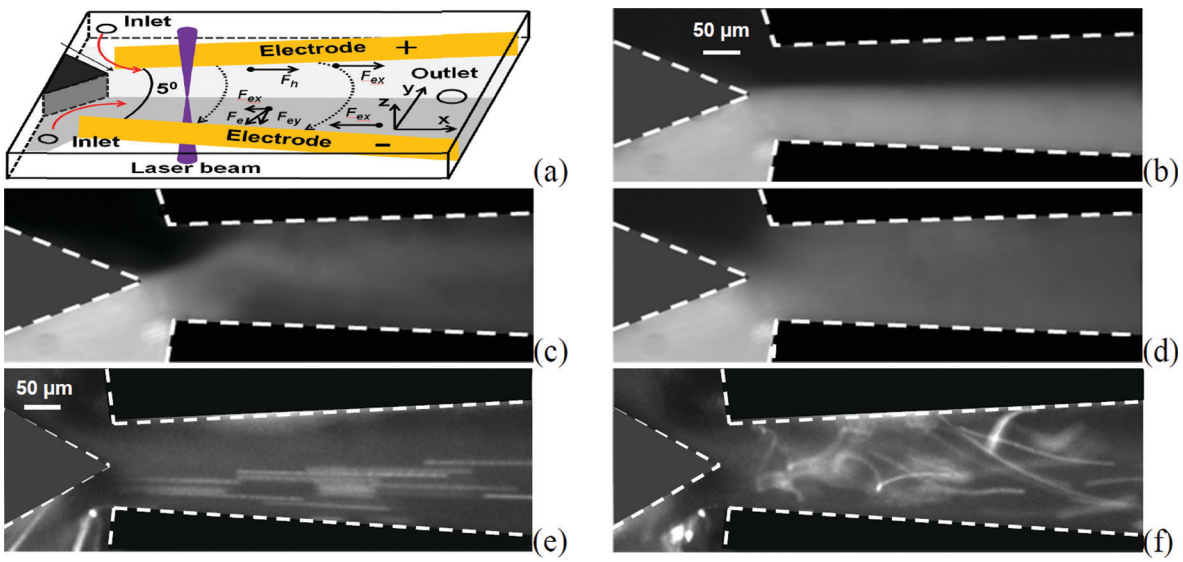

Fig. 1 (a) Schematic of the microfluidic chip setup. The dashed arrow lines represent the instantaneous electric field. (b–f) Visualization of the diffusion process using Laser-Induced Fluorescence. (b) Flow without forcing. The top flow stream is pure buffer solution and the bottom stream is a dye solution. (c) Forcing under 8 V_{p-p}. (d) The flow becomes turbulent, and the diffusion is dramatically enhanced when forced at 20 V_{p-p}. (e) Visualization of the flow (b) with polystyrene particles of 1 μm in diameter. The particles are premixed only with the bottom stream. Straight pathlines indicate that the flow is laminar. (f) The corresponding violent vortex motion of the particles with various sizes of vortices for the flow of (d). The curved pathlines display the random vortices in the flow. The camera exposure time was 0.1 s.

is a relatively sharp trailing edge at the entrance of the microchannel to generate a sharp interface with high conductivity gradient between the two streams. These three methods are novel. (4) Furthermore, $\nabla\sigma$ is significantly enhanced by increasing the conductivity ratio between the two streams up to 5000 : 1. This is much higher than those used in other publications.[22,24] In addition, we also developed a velocimeter that can measure turbulence in microfluidics.

The next challenge is how to measure and characterize turbulent flows in microfluidics using a spatiotemporal resolved velocimeter if there is turbulence in the microchannel. Apparently there is currently no available technique that can measure turbulence in microfluidics.[8] Well-known Micro Particle Imaging Velocimetry (μPIV)[25] could have difficulty in measuring statistical properties of turbulence continuously at a small flow region with high-frequency and strong fluctuations, *e.g.* about 1 kHz in the present work (see Fig. 4). The Laser Doppler Velocimeter (LDV)[26] suffers from spatial resolution (~200 nm is required for the present study) while a hot-wire anemometer (HWA)[27] is invasive and sensitive to electric field and difficult to use in a microchannel for point measurement away from the walls. Other molecular tagging velocimetries[28] also have low temporal resolution. To enable turbulence measurement in microfluidics, a velocimeter having ultrahigh spatiotemporal resolution is required. Correspondingly we have recently developed a molecular tracer based confocal submicroscopic and even nanoscopic velocimeter, *i.e.* the Laser Induced Fluorescence Photobleaching Anemometer (LIFPA)[29–31] to measure the microflow velocity with unprecedented ultrahigh spatiotemporal resolution required for turbulence measurements. The principle of a LIFPA is given in detail in these publications and is similar to that of a HWA, although the former is a noninvasive optical method. Similar to the single wire of a HWA, the LIFPA mainly measures the magnitude of velocity. Hence, if the flow is not unidirectional, the measured signal should be the norm of two components of velocity, *i.e.* u (streamwise component) and v (transverse component). This will still enable us to measure turbulence as a HWA did in its early stage. In the present work, we use our home developed confocal LIFPA to measure turbulence in microfluidics.

3. Experimental system

A schematic of the setup used for the experiment is shown in Fig. 1(a). A microchannel, 240 μm in height and 130 μm in width at the entrance, with a total length of 5 mm was fabricated. The two streams from the entrance of the quasi T-channel are separated by a splitter plate and meet at its trailing edge. The sidewalls of the channel, which have a small divergent angle of 5°, are electrically conductive. Two streams of fluids having fluorescent dye solution and different conductivities were delivered to the microchannel. The conductivity ratio of the two streams is 5000 : 1. A function generator was used to provide the AC electric signal at forcing frequency f_f = 100 kHz (except the case in Fig. 6) with 180° phase shift and various amplitudes to the two electrodes in the microchannel.

To measure the flow velocity using a LIFPA, only a small molecular dye solution of coumarin 102 with the same concentration of 20 μM was used for the two streams, given that there are no fluorescent particles in the flow. The dye molecules are so small that the slip between water and dye can be negligible, and the completely dissolved solution has approximately the same velocity as the dye molecules. To observe intuitively how fast the turbulent mixing is, visualization using a scalar dye, *i.e.* fluorescein sodium, was applied and premixed only in one stream that has high conductivity. To see the existence of vortices in the flow, polystyrene microparticles were used for visualization. The corresponding dielectrophoresis (DEP) effect on particle motion may exist but should not be the major cause of the vortex motion observed, since the bulk velocity caused by pressure difference and convection velocity generated by the electrokinetic force are relatively high. Another reason is that DEP is proportional to the third power of the particle diameter, and the particle diameter used is not larger than 1 μm.

A continuous wave laser (405 nm in wave length) was used as the excitation source. The beam was expanded and then focused to the detection point by an objective (PlanApo, NA 1.4 oil immersions, Olympus, NY). The fluorescence signal was captured using a photomultiplier. To reduce shot and bias noise at the high-frequency regime, suitable cut-off frequencies (the frequency of the low-pass filter for the current preamplifier) f_{sc} are selected. The spatial resolution was approximately determined from the focused laser beam volume that is cylindrical. The diameter and length of this detection volume are determined by diffraction limit and are estimated to be approximately 203 nm and 812 nm, respectively.

4. Experimental results

4.1 Fast diffusion

Fig. 1 shows the fast diffusion feature without and with AC forcing, when Re (Re = UD/ν, where U, D and ν are the bulk flow velocity, the hydraulic diameter and the kinematic viscosity) at the entrance is 0.4 without forcing. Fig. 1(b) shows the case without forcing. Clearly, the flow is laminar and there is almost no mixing except for the negligible molecular diffusion at the interface between the two streams. With forcing at V = 8 V_{p-p}, mixing is decidedly enhanced but not very dramatically, as shown in Fig. 1(c). However, at V = 20 V_{p-p}, the mixing becomes extraordinarily fast even near the entrance, as shown in Fig. 1(d), where the mixing is so rapid that the visualization cannot display the correspondingly detailed kinematic process. Apparently this indicates that there are relatively strong disturbances and vortex motions in the flow, which cause large convection in the transverse direction between the two electrodes. Note that in Fig. 1(d), a little upstream of the trailing edge, there is no mixing at all. Hence, the flow seems to undergo a sudden transition from

laminar to turbulent motion once the two streams converge. After merely 65 μm downstream of the entrance, the concentration almost becomes uniform (at least on a "large scale") in the entire y-direction. The mixing time on a large scale under forcing is estimated to be about 33 ms, nearly 10^3 times faster compared to that only by molecular diffusion in the unforced case. Normally, such a rapid mixing only happens in turbulence. Another feature of turbulence is that there are vortices of different scales. These vortices can also be visualized using polystyrene particles as tracers as shown in Fig. 1(e) and (f). The conditions are consistent with Fig. 1(b) and (d), respectively. Vortices of different sizes can be clearly found in Fig. 1(f), which corresponds to the flow of Fig. 1(d).

4.2 High dissipation

A high turbulent diffusion rate is normally accompanied with high turbulent dissipation caused by viscous shear stresses at small scales. In macroflows, right beyond Re_c, the turbulent dissipation (or pressure drop) will increase rapidly and nonlinearly. Since turbulent kinetic energy will be eventually dissipated, we used the turbulent energy $T_e = \langle u'_s{}^2 \rangle$ to represent the dissipation features equivalently and qualitatively, where $u_s = \sqrt{u^2 + v^2}$ is the instantaneous velocity measured using a LIFPA (u and v are the instantaneous velocity components in the streamwise (x) and transverse (y) directions, respectively, $u'_s = u_s - \langle u_s \rangle$ and "$\langle\ \rangle$" indicates ensemble averaging). Since it is the electrokinetic force that causes the turbulence and corresponding high dissipation, the relationship between T_e and the electric Rayleigh number ($Ra_e = \varepsilon w^2 E_0{}^2(\sigma_2 - \sigma_1)/\sigma_1 \eta D_e$, where w = 130 μm, $\varepsilon = 7.1 \times 10^{-10}$ F m^{-1}, $\eta = 10^{-3}$ kg m^{-1} s^{-1}, $D_e = 1.5 \times 10^{-9}$ m^2 s^{-1}) is used to describe the feature of dissipation in the flow as shown in Fig. 2. As V varies from 0 V_{p-p} to 20 V_{p-p}, E_0 changes from 0 to 1.1×10^5 V m^{-1}.

It can be seen that the critical value of Ra_e, *i.e.* Ra_{ec}, is located between 1.9×10^7 and 4.3×10^7, below which T_e increases slowly with a log–log slope of 0.16. However, beyond the critical point, T_e increases much faster. The slope is estimated to be about 3.03, which is 19 times larger than that of the laminar regime. The relationship between T_e and Ra_e is very similar to that between pressure drop and Re around the transitional regime in macroflows. Fig. 2 indicates that, in general, as Ra_e is increased, the forced microflow also has a dramatically nonlinear increase in dissipation in the turbulent flow compared with that of the laminar flow. Fig. 2 shows the typical transition behavior around $Ra_e = 2.5 \times 10^7$ and a high dissipation feature of turbulence at $Ra_e = 4.7 \times 10^8$.

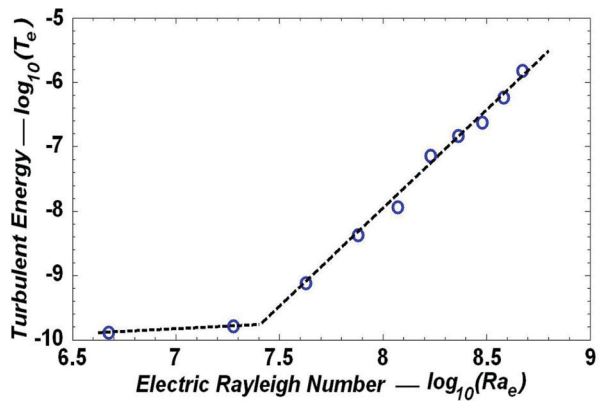

Fig. 2 Relationship between turbulent energy T_e and Ra_e. Data are measured at $y = 0$, $z = 0$ and x_3 = 100 μm.

4.3 Irregularity

Another feature of turbulence is the irregularity, which can be characterized by a time trace of velocity at a fixed spatial point. Time traces of u_s in Fig. 1(b)–(d) at x_3 = 100 μm (the streamwise position is evaluated from the trailing edge) are recorded in Fig. 3. Without forcing, u_s is almost constant. With forcing of V = 8 V_{p-p}, u_s has small fluctuations. In this case, u_s already shows some slight irregularity, but not strong. However, as V is further increased to 20 V_{p-p}, the flow pattern becomes quite different, and u_s is highly fluctuated and random. Note that the forced u_s is much higher than the unforced one, because what the LIFPA measured directly is the magnitude of velocity, which includes the additional contribution from the spanwise velocity component v.

4.4 Multiscale eddies

An intrinsic feature in turbulence is the multiscale eddies that can be described in the spectral space by a power spectrum density $E(f)$ of u_s, where f is the fluctuation frequency of u_s. $E(f)$ without and with different V at various streamwise positions are given in Fig. 4. At x_2 = 10 μm, without forcing, $E(f)$ is nearly flat as background noise, since there is no fluctuation of u_s. The reason that $E(f)$ at low frequency is not completely flat could be due to the vibration of the pump. With forcing of V = 8 V_{p-p}, $E(f)$ at x_2 has significantly

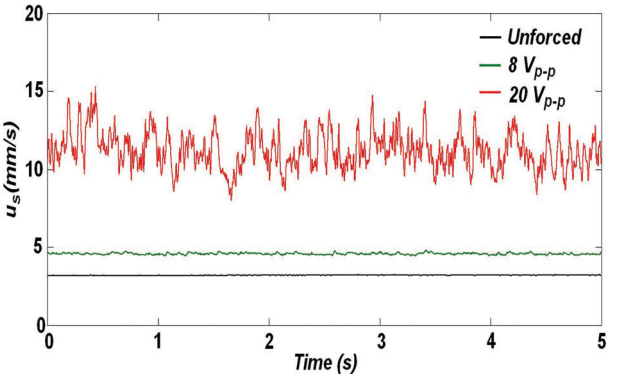

Fig. 3 Time series of u_s at position x_3 = 100 μm, $y = 0$ and $z = 0$. Based on the measured calibration curve between flow velocity and fluorescence intensity, the measured mean velocity of u_s is about 11.2 mm s^{-1}, *i.e.* 5.3 times larger than the unforced bulk velocity U. Therefore, Re based on this forced mean u_s and the hydraulic diameter of the channel at x_3 is about 2.

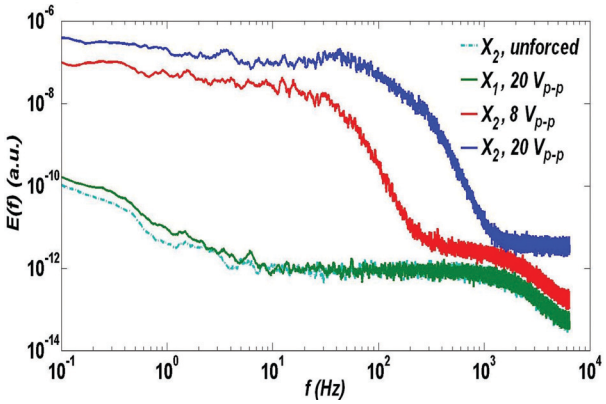

Fig. 4 $E(f)$ of u_s under different voltages and streamwise positions. $E(f)$ without and with forcing under different V (8 and 20 V_{p-p}) at x_2 = 10 μm display significantly different behaviors.

increased. However, $E(f)$ at high f, *e.g.* 100 Hz, that corresponds to "small" scale eddies, is relatively weak.

As V is further increased up to 20 V_{p-p} at x_2, with $E(f)$ at high f, the bandwidth and cut-off frequency f_c of $E(f)$, where noise starts to dominate, also increase both rapidly and significantly. However, at x_1 = −10 μm, $E(f)$ under forcing at V = 20 V_{p-p} is similar to that without forcing, indicating that the flow is still laminar just 10 μm upstream of the inlet. This again indicated a possible sudden transition from laminar to turbulent flow. Note that there is no sharp peak for $E(f)$ at 100 kHz, although the forcing frequency f_f is 100 kHz and the temporal resolution of the LIFPA are sufficient to measure a 100 kHz signal when both the sampling rate and f_{sc} are 1 MHz. In particular, while f_c at V = 8 V_{p-p} is about 200 Hz, it increases approximately to 1.5 kHz at V = 20 V_{p-p}. This could indicate that the forcing at V = 20 V_{p-p} generates velocity fluctuations that produce relatively "large scale" eddies, which in turn produce small scale eddies down to dissipation scale l_{de}, where the viscous force dominates. The energetic large velocity fluctuations also induce higher dissipation rate and smaller eddies. This could explain why f_c moves toward the high frequency regime under forcing of V = 20 V_{p-p}, compared to that under forcing of V = 8 V_{p-p}. At V = 20 V_{p-p}, within 3–60 Hz, $E(f)$ is almost constant and about four orders of magnitude higher than that of the unforced flow. Furthermore, although $E(f)$ continuously decreases with the increasing of f beyond about 60 Hz at a slope of approximately −5/3 (note that turbulence does not always require the existence of −5/3 inertial range of high Re turbulence, and many macro turbulent flows do not have the inertial range in the spectrum), it does not fall sharply. Only when f is higher than 300 Hz did $E(f)$ start to decay sharply with a slope of about −5. Since the velocity power spectrum with V = 20 V_{p-p} decays much slower than f^{-3} in the range from 1 to 300 Hz, Fig. 4 could exclude the possible temporally random but spatially smooth chaotic flow normally observed at very low Re, which requires $E(f)$ to decay faster than f^{-3}.[32,33] Hence, although it is not clear if the flow forced at V = 8 V_{p-p} is turbulent or not, the flow forced at V = 20 V_{p-p} should be turbulent, considering that there are multiscale eddies corresponding to the wide bandwidth from 1 to 300 Hz, where $E(f)$ has no sharp decrease, another typical feature of turbulence.

4.5 Continuity

To evaluate the continuity of the flow, we use Knudsen number, *i.e.* the ratio of mean free path ξ of water to the estimated smallest structure l_{de}, as the criterion.[16] Based on Fig. 4, the l_{de} corresponding to the forced flow at V = 20 V_{p-p} is estimated to be about 0.2–1 μm. ξ is about 0.02 nm.[17] Thus, the ratio $\xi/l_{de} \ll 1$. This confirms that the flow in Fig. 1(d) is still continuous, although the channel's size is in microscale.

4.6 3-D flow

The 3-D nature of instant flow is a basic feature of turbulence. Actually, the inhomogeneity of flow in the x-direction is apparent from both Fig. 1(d) and 4. What we need is to measure the inhomogeneity in the y–z plane. For this purpose, the distributions of T_e along the transverse y-direction were measured at two different z-positions (spanwise) at downstream (x_3 = 100 μm), as shown in Fig. 5. While T_e in the unforced flow (caused by the low frequency noise, such as pump vibration and negligible shot noise) is very small and negligible, T_e in the forced flow at V = 20 V_{p-p} is increased by 3–4 orders, and the flow becomes highly fluctuated and 3-D. From Fig. 5, it can be found that for y = 0 μm in the z-direction, T_e at z = 0 μm is about 2.7 times larger than that at z = −100 μm. For z = 0 μm in the y-direction, T_e at y = 0 μm is about 30 times higher than that at y = 30 μm. The variation of T_e in the y-direction is much larger than that in the z-direction. This is reasonable as the flow disturbance is generated by $\vec{F}_e = -\frac{\varepsilon \vec{E}\cdot\nabla\sigma}{\sigma}\vec{E}$, and $\nabla\sigma$ is maximum at the centerline in the y-direction. It implies that the local ratio of electrokinetic force

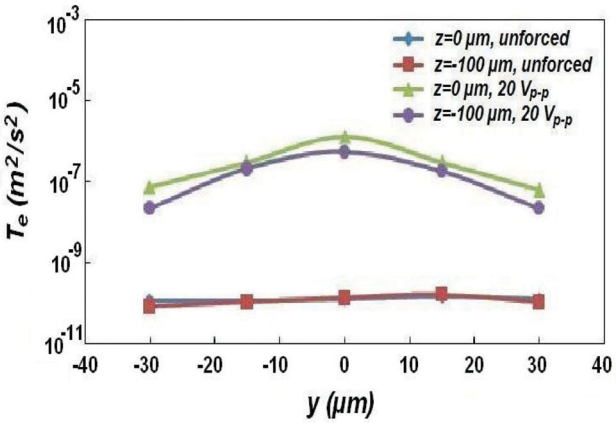

Fig. 5 T_e distribution along the transverse direction at two vertical positions without and with forcing of V = 20 V_{p-p} at x_3 = 100 μm.

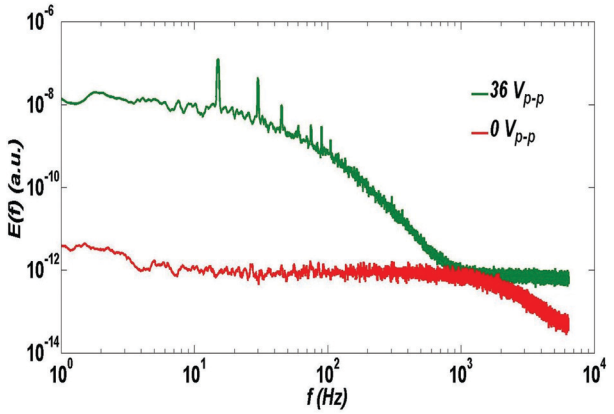

Fig. 6 $E(f)$ with low forcing frequency of 15 Hz at position x_3 = 100 μm. Compared with the unforced one, the $E(f)$ of the forced one is much higher at frequency from 10 Hz to 500 Hz.

to viscosity force, *i.e.* Gr_e, changed much faster in the y-direction than in the z-direction, which is due to the 3-D variation of conductivity structures. This indicates the intrinsic 3-D nature of the flow.

5. Discussion

Since rapid time periodic forcing (100 kHz) is used to force the flow, it is not clear whether the large scale structures (low frequency signals) and small structures (high frequency signal) in Fig. 4 resulted from viscous damping of much smaller scale structures (*i.e.* a much higher frequency signal), with f_f = 100 kHz. If this is true, then what we have in Fig. 4 could not be turbulence, but actually a chaotic flow and mixing generated in a 3-D geometry through viscous diffusion of the forced smaller structures produced at high f_f. To address this issue, we first recall what Ottino (1990) mentioned, "It is simplistic to seek a clean answer to the questions of whether turbulence is chaotic or chaos is turbulent". We need to make it clear that studying the difference between chaotic flow and turbulence, a difficult topic, is out of the scope of the present work. To ensure that spectrum $E(f)$ in Fig. 4 with V = 20 V_{p-p}, including the large scale low frequency and small scale high frequency signals, is not just the consequence of the viscous damping of the higher frequency signal at such a low Re flow, we first measured the $E(f)$ with f_{sc} = 1 MHz for the flow in Fig. 1(d) and found no signal at all, but noise was detected at 100 kHz although the flow was forced at this frequency. For such a high f_{sc}, the noise is higher than that in Fig. 4, because shot noise increases with frequency.[34] Then, forcing at a low f_f of 15 Hz is also investigated to ensure that $E(f)$ has both high and low frequency signals without high f_f.

As electrolysis could create bubbles at such a low f_f, we reduced the conductivity ratio to 10 and increased the forcing voltage V to 36 V_{p-p}. Ra_e is about 2.8×10^6 in this case. Nevertheless, the principle of generating turbulence in this type of flow is similar for all f_f used. The result is shown in Fig. 6, where f_c is still about 1 kHz, more than sixty times of f_f. Fig. 6 indicates that the $E(f)$ generated at f_f = 15 Hz is similar to that at f_f = 100 kHz qualitatively. The length scale estimated from f_f and bulk velocity, *i.e.* U/f_f, is in the same order of the channel width. Therefore, in this case, both low and high frequency signals in $E(f)$ should not be created by viscous damping of the higher frequency signal, but probably because of the loss of flow stability under strong forcing and turbulence. In fact, our experiment also finds that this type of flow normally becomes more unstable at lower f_f, and the lower the f_f, the more unstable the flow for a given voltage. The reason we select the high frequency is mainly because of its potential future application in lab-on-a-chip to avoid the possible bubble generation at a low frequency.

In macroflows, low Re elastic turbulence has been reported,[1] where the fluid has to be a polymer, but no elastic turbulence has, to the best of our knowledge, been reported in microfluidics. In the present work, the fluid is not non-Newtonian, but common Newtonian, *i.e.* water solution with small ions. Electrokinetic forcing has also widely been applied in microfluidics. However, no publication has claimed that turbulence flow has been observed in Re below 10 in electrokinetically forced flows with a Newtonian fluid. Burghelea *et al.*[8] reported that the most popular velocimeter, μPIV, has difficulty in exploring the properties of the flow down to sufficiently small spatial scales about its spatial structure because of its limited resolution. Here we have not only used a unique method to generate turbulence but also developed a new method to be able to measure turbulence in microchannels. Since the origin of the transition to turbulence is not mainly because of the pressure driven pipe or channel macroflows, but the electrokinetic forcing in the microchannel, we name the flow as micro electrokinetic turbulence (or μEK turbulence) to distinguish it from "micro turbulence" used already in other fields.[35,36]

6. Conclusion

The studied electrokinetically forced flow at sufficiently high electric field virtually has all of the features of turbulence, which are classically used as criteria to determine if a flow is turbulent, except the Reynolds number is not high. Therefore, the present work demonstrates that increasing the electric Rayleigh number can overcome the viscous effect to generate turbulence, although the Reynolds number is very low in microfluidics. This discovery may provide a new perspective on turbulence, a novel opportunity for flow manipulation and control in microfluidics at low Re and insight into transport phenomena in micro- and nanoscale in life science.

Acknowledgements

We appreciate discussions with Chih-Ming Ho and Patrick Tabeling. The work was supported by the NSF under grant no. CAREER CBET-

0954977, MRI CBET-1040227 and SC EPSCOR/IDEA GEAR award respectively.

References

1 A. Groisman and V. Steinberg, *Nature*, 2000, **405**, 53–55.
2 A. D. Stroock, S. K. W. Dertinger, A. Ajdari, I. Mezić, H. A. Stone and G. M. Whitesides, *Science*, 2002, **295**, 647–651.
3 D. Janasek, J. Franzke and A. Manz, *Nature*, 2006, **442**, 374–380.
4 Y.-C. Ahn, W. Jung and Z. Chen, *Lab Chip*, 2008, **8**, 125–133.
5 L. Capretto, W. Cheng, M. Hill and X. Zhang, *Top. Curr. Chem.*, 2011, **304**, 42.
6 C. Simonnet and A. Groisman, *Phys. Rev. Lett.*, 2005, **94**, 134501.
7 S. Balasuriya, *Phys. Rev. Lett.*, 2010, **105**, 064501.
8 T. Burghelea, E. Segre, I. Bar-Joseph, A. Groisman and V. Steinberg, *Phys. Rev. E: Stat., Nonlinear, Soft Matter Phys.*, 2004, **69**, 066305.
9 C.-C. Chang and R.-J. Yang, *Microfluid. Nanofluid.*, 2007, **3**, 501–525.
10 M. H. Oddy, J. G. Santiago and J. C. Mikkelsen, *Anal. Chem.*, 2001, **73**, 5822–5832.
11 C.-H. Chen, H. Lin, S. K. Lele and J. G. Santiago, *J. Fluid Mech.*, 2005, **524**, 263–303.
12 H. Hu, Z. Jin, A. Dawoud and R. Jankowiak, *J. Fluid Sci. Tech.*, 2008, **3**, 260–273.
13 M.-Z. Huang, R.-J. Yang, C.-H. Tai, C.-H. Tsai and L.-M. Fu, *Biomed. Microdevices*, 2006, **8**, 309–315.
14 J. Park, S. Shin, K. Y. Huh and I. Kang, *Phys. Fluids*, 2005, **17**, 118101.
15 H. Lin, B. D. Storey, M. H. Oddy, C.-H. Chen and J. G. Santiago, *Phys. Fluids*, 2004, **16**, 1922.
16 H. Tennekes and J. L. Lumley, *A First Course in Turbulence*, The MIT press, 1972.
17 B. Kirby, *Micro- and Nanoscale Fluid Mechanics: Transport in Microfluidic Devices*, Cambridge University Press, 2010.
18 P. Tabeling, *Introduction to Microfluidics*, Oxford University Press, USA, 2010.
19 K. V. Sharp, R. J. Adrian, J. G. Santiago and J. I. Molho, in *The Mems Handbook*, ed. M. Gad-el-Hak, CRC Press, 2002.
20 G. R. Wang, *AIChE J.*, 2006, **52**, 111–124.
21 G. R. Wang, *Chemical Engineering Science*, 2003, **58**, 4953–4963.
22 J. C. Baygents and F. Baldessari, *Phys. Fluids*, 1998, **10**, 301.
23 J. D. Posner and J. G. Santiago, *J. Fluid Mech.*, 2006, **555**, 1–42.
24 A. O. El Moctar, N. Aubry and J. Batton, *Lab Chip*, 2003, **3**, 273–280.
25 J. G. Santiago, S. T. Wereley, C. D. Meinhart, D. J. Beebe and R. J. Adrian, *Exp. Fluids*, 1998, **25**, 316–319.
26 Y. Zhao, Z. Chen, C. Saxer, S. Xiang, J. F. de Boer and J. S. Nelson, *Opt. Lett.*, 2000, **25**, 114–116.
27 C. Liu, J.-B. Huang, Z. Zhu, F. Jiang, S. Tung, Y.-C. Tai and C.-M. Ho, *J. Microelectromech. Syst.*, 1999, **8**, 90–99.
28 H. Hu and M. M. Koochesfahani, *Meas. Sci. Technol.*, 2006, 1269.
29 C. Kuang, R. Qiao and G. Wang, *Microfluid. Nanofluid.*, 2011, **11**, 353–358.
30 C. Kuang and G. Wang, *Lab Chip*, 2010, **10**, 240–245.
31 C. Kuang, W. Zhao, F. Yang and G. Wang, *Microfluid. Nanofluid.*, 2009, **7**, 509–517.
32 A. Fouxon and V. Lebedev, *Phys. Fluids*, 2003, **15**, 2060–2072.
33 T. Burghelea, E. Segre and V. Steinberg, *Phys. Rev. Lett.*, 2004, **92**, 164501.
34 G. R. Wang and H. E. Fiedler, *Exp. Fluids*, 2000, **29**, 10.
35 C. D. Jager, *Nature*, 1954, **173**, 680–681.
36 W. W. Heidbrink, J. M. Park, M. Murakami, C. C. Petty, C. Holcomb and M. A. Van Zeeland, *Phys. Rev. Lett.*, 2009, **103**, 175001.

